*Article*

# Morphological, Structural and Hydrogen Storage Properties of LaCrO$_3$ Perovskite-Type Oxides

**Mohamed Amine Lahlou Nabil [1,2], Nouredine Fenineche [1,2,*], Ioana Popa [3] and Joan Josep Sunyol [4]**

[1] ICB-PMDM, UBFC University, UTBM, Rue du Leupe, CEDEX, 90040 Sevenans, France; mohamed.lahlou-nabil@utbm.fr

[2] FR FCLAB, UTBM bât. F, Rue Thierry Mieg, CEDEX, 90010 Belfort, France

[3] ICB, UMR CNRS 6303, UBFC University, 9 Av. Alain Savary, CEDEX, 21078 Dijon, France; ioana.popa@u-bourgogne.fr

[4] Department de Fisica, Campus Montilivi, Universitat de Girona, 17071 Girona, Spain; joanjosep.sunyol@udg.edu

[*] Correspondence: nour-eddine.fenineche@utbm.fr

**Abstract:** Recently, perovskite-type oxides have attracted researchers as new materials for solid hydrogen storage. This paper presents the performances of perovskite-type oxide LaCrO$_3$ dedicated for hydrogen solid storage using both numerical and experimental methods. Ab initio calculations have been used here with the aim to investigate the electronic, mechanical and elastic properties of LaCrO$_3$H$_x$ (x = 0, 6) for hydrogen storage applications. Cell parameters, crystal structures and mechanical properties are determined. Additionally, the cohesive energy indicates the stability of the hydride. Furthermore, the mechanical properties showed that both compounds (before and after hydrogenation) are stable. The microstructure and storage capacity at different temperatures of these compounds have been studied. We have shown that storage capacities are around 4 wt%. The properties obtained from this type of hydride showed that it can be used for future applications. XRD analysis was conducted in order to study the structural properties of the compound. Besides morphological, thermogravimetric analysis was also conducted on the perovskite-type oxide. Finally, a comparison of these materials with other hydrides used for hydrogen storage was carried out.

**Keywords:** perovskite-type oxide; hydrogen storage; XRD analysis; rietveld refinement; ab initio calculations

## 1. Introduction

Hydrogen represents a clean source and very important energy vector. Hydrogen has always been the focus of related research because of the high value of its energetic density. Hydrogen is primarily produced using two principal methods: steam reforming and electrolysis. Steam reforming is a high-temperature process in which steam reacts with hydrocarbon fuel to produce hydrogen. In order to produce hydrogen, there is a high-temperature process where steam reacts with hydrocarbon fuels called steam reforming. Moreover, hydrogen can also be produced by reforming hydrocarbon fuels, such as natural gas, diesel, renewable liquid fuels and gasified cool or gasified biomass. Currently, 95% of hydrogen is produced by steam reforming of natural gas. Electrolysis is a process that splits water into hydrogen and oxygen using an electric current. Hydrogen is an efficient way to store and transport energy. Hydrogen is also used for electricity production through a fuel cell which produces electricity by converting chemical energy into electrical energy. Using hydrogen does not emit greenhouse gases, offering a potential solution for pollution issues. Storing hydrogen is necessary to palliate the renewable energy intermittency and has multiple uses. It acts as energy source for land, sea and rail transport, enabling greater fuel endurance, quick refueling and zero harmful emissions. The most-used techniques to store hydrogen are gaseous, liquid hydrogen or solid-state hydrogen in materials. Gaseous hydrogen storage mode has become a widely used hydrogen storage method due to its

technical simplicity and rapid filling and release kinetics. However, when the hydrogen storage pressure is lower than 20 MPa, the volumetric hydrogen density of this significantly increases the energy consumption for compression and the tank cost. Solid hydrogen storage represents an important economic issue and is nowadays a promising technology for fuel cells vehicles since the volumetric hydrogen density of materials is usually higher than 100 Kg/m$^3$. Therefore, smaller tanks can be used to store large amounts of hydrogen [1–18].

Among the different families of intermetallic compounds, we can cite: AB, AB$_2$, A$_2$B, A$_2$B$_7$ and AB$_5$. Where A and B are two elements with high storage capacity and low affinity with H2, respectively. AB$_5$-type intermetallic compounds, in particular LaNi$_5$-based alloys, are the most studied compounds for Ni/MH batteries. However, the high production cost of Lanthanum slow their application in commercial devices [19–21]. Over the past decade, rare earth perovskite AB$_3$ type oxides have attracted the attention of researchers as new materials for hydrogen storage. These have been considered one of the most valuable alternatives for hydrogen solid storage. Traditionally, perovskite materials have an ABX$_3$ structure, where A and B are cations and X is an anion. Magnesium-based perovskite-type hydrides have received special attention from researchers due to their high hydrogen storage capacity. Indeed, Lefevre et al. [22] investigated the hydrogen storage capacity of MgNi$_3$H$_2$ and MgCuH$_3$ using ab initio calculations. It was shown that these alloys are stable and may be used for transportation applications. Moreover, Reshak et al. [23] carried out a study on the structural, elastic and electronic properties of the perovskite KMgH$_3$. In addition, CaNiH$_3$ perovskite hydrides are also considered for hydrogen storage and Ikeda et al. [24] reported similar desorption characteristics, and the hydrogen desorption of CaNiH$_3$ is higher than that of CaCoH$_3$. This interest is due to their abundance, thermal resistance and lower cost compared to conventional intermetallic alloys. Magnesium-based perovskites, such as NaMgH$_3$, were of particular interest due to their large hydrogen storage capacity [25–27]. In addition, perovskite hydrides of the CaNiH$_3$ type have been studied for the storage of hydrogen.

In order to study the performance of perovskite oxides for hydrogen storage, several studies were carried out at room temperature. Sakaguchi et al. [28] were the first to study perovskites (SrCe$_{0.95}$Yb$_{0.05}$O$_3$) for Ni/MH batteries. They have shown that these perovskites are able to store hydrogen at room temperature. Subsequently, Esaka et al. [29] proposed another perovskite as a battery electrode having the composition ACe$_{1-x}$M$_x$O$_{3-d}$ (A = Sr or Ba, M = rare earth element). It was found that the latter successfully stored hydrogen and could undergo electrochemical charging and discharging of hydrogen at room temperature. Despite these successful results, the maximum capacity was estimated at 119 mAh/g which is significantly lower than that of AB$_5$ type alloys at room temperature.

Furthermore, Deng et al. [30] investigated the electrochemical hydrogen storage properties of perovskite-type oxide LaCrO$_3$ as negative electrode for Ni/MH batteries and showed excellent electrochemical reversibility and considerably high charge–discharge capacity at various temperatures up to 285 mA h g$^{-1}$.

In their study, Gencer et al. [31] were interested in the study of the compounds MgTiO$_3$H$_x$ and CaTiO$_3$H$_x$ (x = 0, 3, 6, and 8). Among all these compounds, the only good candidate for storage is CaTiO$_3$H$_6$ due to its stability and its good storage capacity, which is 4.27 wt%.

The aim of the present work is to study the hydrogen storage properties of the perovskite-type oxide LaCrO$_3$, as there is no experimental study in the literature on perovskite-type oxide materials for hydrogen solid storage, with the exception of the perovskite hydrides mentioned above and the numerical study of Gencer et al. [31]. In this study, a double approach is carried out. A numerical approach consisting of studying the system LaCrO$_3$ before and after restitution of hydrogen atoms by using ab initio calculations. An experimental approach focusing on the elaboration of the perovskite type oxide; then, a structural and morphological characterization is carried out before measuring the storage capacities. Therefore, the present paper presents the perovskite-type oxide LaCrO$_3$ as a novel material dedicated for hydrogen storage.

## 2. Numerical Methods and Experimental Details

### 2.1. Computational Detail

In the present work, the full potential (FP-LAPW) method is used within the density functional theory (DFT) [32,33]. Electron exchange correlation energy is described in the generalized gradient approximation (GGA) using the Perdew–Burke–Enzerhof functional parameterization [34]. The expansion of basic functions, potentials and electron densities inside the muffin-tin spheres in combination with spherical harmonic functions with a cut off Lmax = 10, and in Fourier series in the interstitial region. The parameter RMT Kmax = 4.0 serves to determine the matrix size, where RMT denotes the smallest atomic sphere radius and Kmax determines the magnitude of the largest K vector in the plane-wave expansion. All the calculations were carried out at the theoretical equilibrium lattice constants. Values of 2.17, 2.13, 1.92 and 0.71 a.u. are the values of the muffin-tin radii [35] of La, Cr, O and H, respectively. The K Integration over the Brillouin zone is performed using the Monkhorst–Pack scheme with 2000 K-points in the Brillouin zone. The self-consistent calculations are considered to be converged only when the calculated total energy of the crystal is converged to less than 0.1 mRyd.

### 2.2. Material Preparation and Characterization

Lanthanum chromite $LaCrO_3$ was synthesized using the Pechini sol-gel method. The precursors $La(NO_3)_3 \cdot 6H_2O$, (98.5% purity, Alfa Aesar) and $Cr(NO_3)_3 \cdot 9H_2O$, (99.9% purity, Alfa Aesar) were firstly weighted at the stoichiometric ratio La:Cr of 1:1 and dissolved in a solution of citric acid, followed by the addition of ethylene glycol in a molar ratio of citric acid: ethylene glycol 1:4 to form a polymeric resin. The solution was then heated on a thermal plate under constant stirring at 130 °C to promote polymerization and to allow solvent removal. A viscous gel was thus obtained. The temperature was subsequently raised at 10 °C/min rate up to 300 °C to assure the propagation of combustion which transforms the gel into a fine powder. Finally, the obtained powder was grounded in a mortar then calcined at 800 °C in air.

Crystallographic analysis of the bulk sample was carried out by X-ray diffraction (XRD) at room temperature using a BRUKER D8 Advance diffractometer in a θ–2θ Bragg Brentano geometry using Cu Kα radiation ($\lambda_{\alpha Cu}$ = 0.154056 nm). The crystalline phase present in the sample was performed using EVA program (Bruker-AXS). The corresponding structural parameters were determined by Rietveld refinement carried out using the MAUD [36]. Scanning electron microscopy measurements were performed on DSM960A Zeiss field emission scanning electron microscope (FE-SEM). In order to determine the calcination temperature, thermogravimetric analysis (TGA) and differential thermal analysis (DTA) of $LaCrO_3$ solid precursor were performed using Mettler Toledo TGA/SDTA851e, by heating from room temperature up to 1000 °C in air with an increment of 10 °C/min.

The homogeneity of the compound was investigated by Energy Dispersive X-ray Spectroscopy (EDS) analysis at different morphological positions of the compound. The size distribution of the particles was obtained from the SEM images using Image J software.

The perovskite-type oxide powder was firstly activated before conducting any hydrogen storage measurements. This step was carried out by repeating three sorption/desorption cycles at 3 bars and at 333 K. The pressure composition temperature (PCT) measurements were conducted using Sieverts type volumetric apparatus supplied by SETARAM (model PCT-Pro). The compound at known pressure and volume is connected to a reservoir of known volume and pressure of hydrogen through an isolation valve. Opening the isolation valve allows new equilibrium to be established. Hydrogen sorption is determined by the difference between the actual measured pressure ($P_f$) and the calculated pressure ($P_c$). The hydrogen absorption and desorption measurements were carried out at three different temperatures up to 333 K.

## 3. Results and Discussion

### 3.1. Numerical Study

Crystal Structure of LaCrO$_3$H$_X$ (x = 0, 6)

LaCrO$_3$H$_6$ also crystallizes in a cubic structure of Fd-3m space group. In this unit cell, La atoms occupy 1b (0.5, 0.5, 0.5) sites, Cr atoms occupy 1a (0, 0, 0) sites, O atoms occupy 3c (0, 0.5, 0.5) and H atoms occupy 6f (0.088, 0.5, 0.5) sites, where 1a, 1b, 3c and 6f are Wyckoff positions given in Table 1. A summary of the crystallographic parameters and atomic positions used in our calculations is presented in Table 1. It must be noted that our calculations are performed with a primitive cell, which contains one formula unit (11 atoms).

**Table 1.** Crystallographic parameters and atomic positions used in our calculations.

| Compound and Space Group | Wyckoff Notation and Positions | | Lattice Parameters |
|---|---|---|---|
| LaCrO$_3$H$_6$ (Fd3m) | 1b | La (0.5,0.5,0.5) | a = b = c 4.43 (Å) |
| | 1a | Cr (0,0,0) | |
| | 3c | O (0.0, 0.5, 0.5) | α = β = γ = 90° |
| | 6f | H (0.088, 0.05, 0.5) | |
| LaCrO$_3$ (Fd3m) | 1a | La (0.5,0.5,0.5) | a = b = c 3.92 (Å) |
| | 1a | Cr (0,0,0) | α = β = γ = 90° |
| | 3c | O (0.0, 0.5, 0.5) | |

### 3.2. Electronic Properties of LaCrO$_3$ and LaCrO$_3$H$_6$

Figure 1a,b represents the total and the partial electronic densities of states (DOS) for LaCrO$_3$ and LaCrO$_3$H$_6$ as a function of energy (eV). The Fermi level is set to zero energy (dotted line). The electronic band structure along the high symmetry directions obtained from the calculated equilibrium lattice constants of LaCrO$_3$ and LaCrO$_3$H$_6$ is shown in Figure 1.



(a)
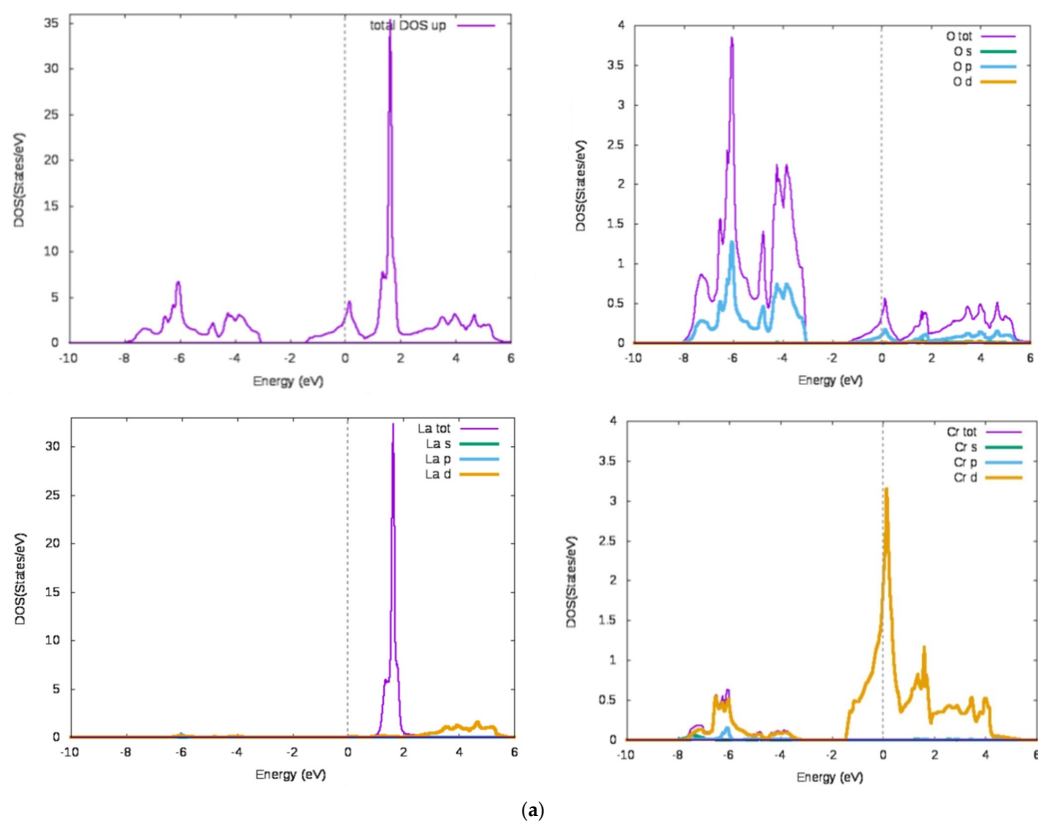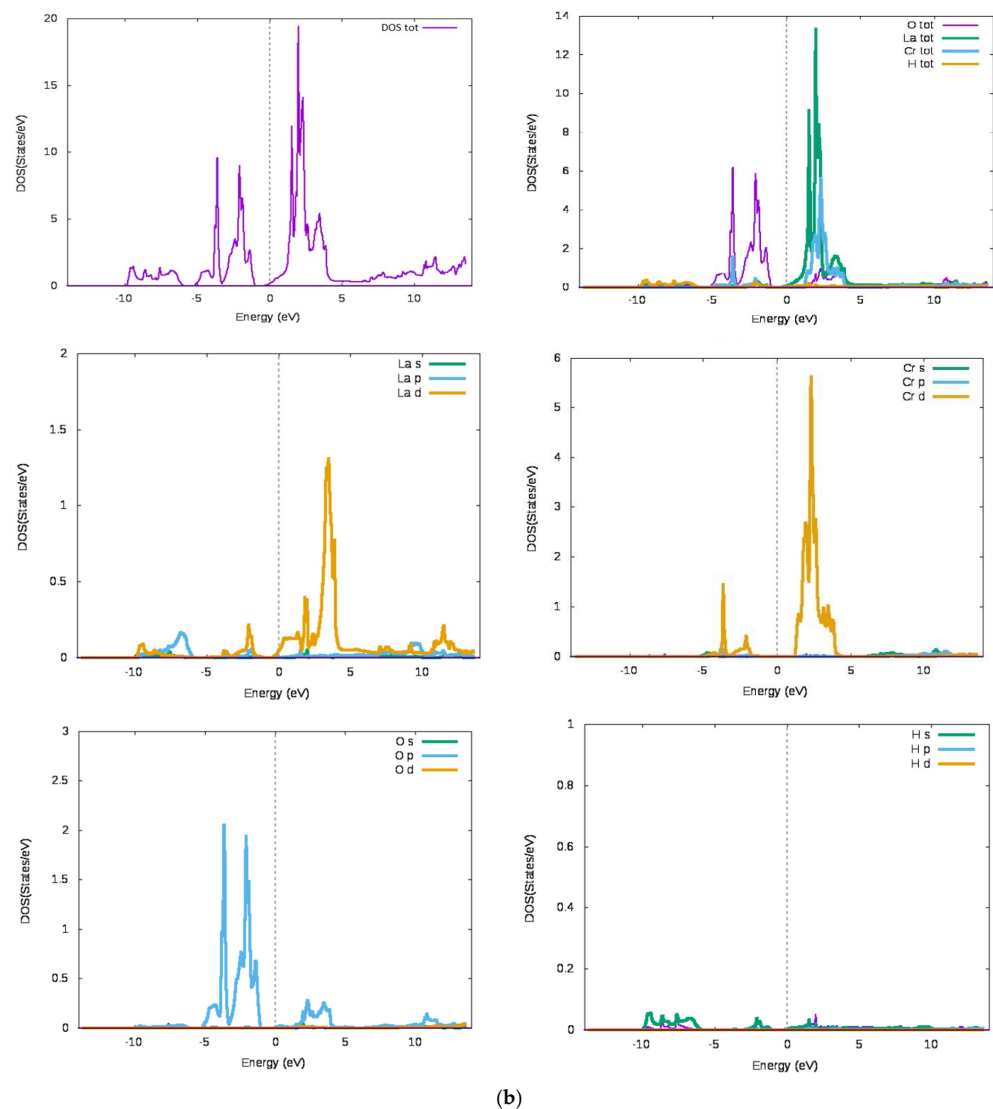
**Figure 1.** *Cont.*

**Figure 1.** (**a**) Representation of the total and partial density of states of LaCrO$_3$. (**b**). Total and partial density of states of LaCrO$_3$H$_6$.

Downstream of the Fermi level, it can be seen that the main contributions are those of O oxygen atoms. Upstream of the Fermi level, the greatest contribution is that of Cr-d and La-d, which determine the total DOS shape. Furthermore, the presence of hydrogen creates additional states, hence the extension of the curve. It can also be noticed that the values of the density of state at the Fermi levels are very low for LaCrO$_3$ and LaCrO$_3$H$_6$, respectively. This character gives the information about the stabilizing effect of electron states on a physical basis. In general, the lower the DOS at the Fermi level, the more stable the compound [37].

### 3.3. Mechanical Properties

In order to obtain the ground state properties, the calculation of the total energies at different volumes is performed around the equilibrium. Then, it is fitted to Murnaghan's state equation (Figure 2) [38]. The evaluated ground state properties, such as cell parameters, bulk modulus B$_0$ and its pressure derivative B$_0'$ are illustrated in Table 2. This evaluation is done by performing an analytical interpolation of the computed points from Birch–Murnaghan fit expressing the variation of total energy versus volume. It can be noticed that LaCrO$_3$ is the most stable when the lowest value of energy is reached ($-1955.14192$ Ry). The deviation of the optimized parameters compared to experimental ones is about 1.81%

for LaCrO$_3$. This deviation is acceptable. Bulk modulus represents the material volume variation under hydrostatic pressure. As can be concluded from Table 2, LaCrO$_3$ has the highest values of bulk modulus, through the studied compounds. Moreover, the obtained results are in good agreement with the available literature results [38,39]. Furthermore, when the hydrogen binds to LaCrO$_3$, the bulk modulus decreases, which means it is easier to compress the material [40].

$$E(V) = E_0 + \frac{9V_0B_0}{16} \left\{ \left[ \left[ \left( \frac{V_0}{V} \right)^{\frac{2}{3}} \right] - 1 \right]^3 B_0' + \left[ \left( \frac{V_0}{V} \right)^{\frac{2}{3}} - 1 \right]^2 \left[ 6 - 4 \left( \frac{V_0}{V} \right)^{\frac{2}{3}} \right] \right\} \quad (1)$$
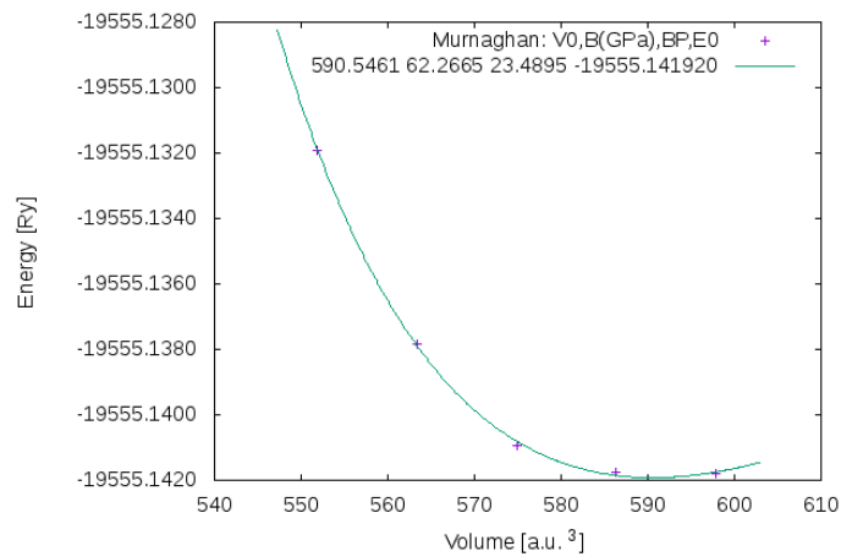


**Figure 2.** Total energy (Ry) vs. unit cell volume for LaCrO$_3$H$_6$.

**Table 2.** Cell parameters, mechanical properties of LaCrO$_3$ and LaCrO$_3$H$_6$.

| Compounds | Reference | Approximation | Calculated Cell Parameters (A) | | | B (GPa) | B' (GPa) |
|---|---|---|---|---|---|---|---|
| | | | a | b | c | | |
| LaCrO$_3$ | Present | GGA | 3.85 | 3.85 | 3.85 | 128.07 | 3.2 |
| | [39] | Experimental | 3.92 | 3.92 | 3.92 | / | / |
| | [41] | GGA | - | - | - | 231 | / |
| LaCrO$_3$H$_6$ | Present | GGA | 4.43 | 4.43 | 4.43 | 62.26 | 23.48 |

*3.4. Cohesive Energy*

The cohesive energy for LaCrO$_3$H$_6$ is calculated in order to study the relative phase stabilities. This latter represents the strength of the forces that bind atoms together in the solid state. The cohesive energy $E_{coh}^{LaCrO_3H_6}$ per atom of LaCrO$_3$H$_6$ is defined as the total energy of the constituent atoms minus the total energy of the compound [42]:

$$E_{coh}^{LaCrO_3H_6} = \frac{\left[ A * E_{atom}^{La} + B * E_{atom}^{Cr} + C * E_{atom}^{H} + D * E_{atom}^{O} \right] - E_{total}^{LaCrO_3H_6}}{A + B + C + D}$$

where:
$E_{coh}^{LaCrO_3H_6}$ is the cohesive energy per atom of LaCrO$_3$H$_6$;
$E_{total}^{LaCrO_3H_6}$ is the total energy of the hydrid LaCrO$_3$H$_6$ in the equilibrium configuration;
$E_{atom}^{La}$, $E_{atom}^{Cr}$, $E_{atom}^{O}$ and $E_{atom}^{H}$ are the isolated atomic energies for pure constituents, while A, B and C are the numbers of La, Cr, O and H atoms in unit cell, respectively.

Then:

$$E_{coh}^{LaCrO_3H_6} = \frac{\left[E_{atom}^{La} + E_{atom}^{Cr} + 3E_{atom}^{O} + 6E_{atom}^{H}\right] - E_{total}^{LaCrO_3H_6}}{11}$$

The calculation of the cohesive energy shows a positive value $E_{coh}^{LaCrO_3H_6} = 0.642$ Ry/atom, which means that the hydride is energetically stable.

### 3.5. Experimental Investigations

In order to determine the calcination temperature allowing for a well-crystalized oxide, the air-dried precursor of $LaCrO_3$ was analyzed by thermogravimetry and differential temperature analysis, TGA and DTA, respectively. Thermal analysis was conducted in order to detect evaporation, oxidation solid-gas reaction and other transformations that involve a mass change that take place when the temperature is changed. Figure 3 shows TGA–DTA curves of the $LaCrO_3$ precursor. The TGA curve might be divided to three parts. For Part A, in the range of 20 °C to 350 °C, we can observe a mass loss of about 16% with an inflection at the temperature of 110 °C, which corresponds to a wide endothermic band. The latter may be due to the remaining water evaporation in the precursor. Part B represents a mass loss of 10% between 360 °C and 700 °C, which corresponds to a large exothermic band at 360 °C. This mass loss can also be explained by citrate decomposition as well as decarboxylation. Part C, between 700 °C and 1000 °C, represents a final mass loss in correlation with an endothermic band located at 800 °C. This process likely corresponds to a loss of oxygen from the reduction of an intermediate lanthanum chromate phase resulting in final generation of the lanthanum chromite perovskite. Beyond 800 °C, no significant weight loss was observed. Therefore, the most adequate calcination temperature is chosen at 800 °C. These results agree with previous results [43].
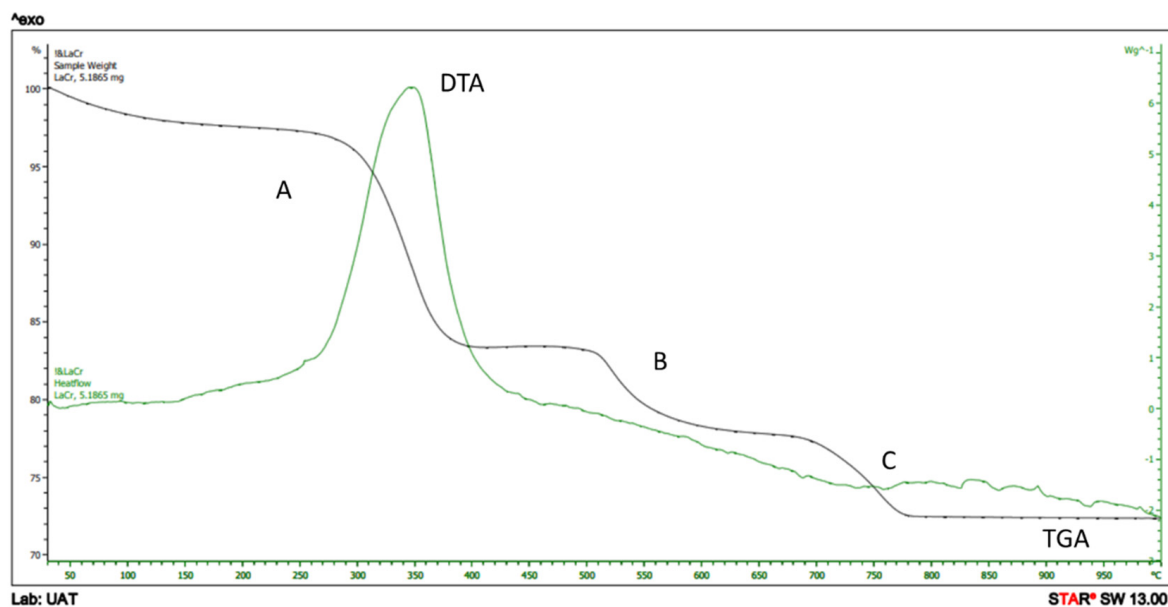


**Figure 3.** TG/DTA curves of the powder precursor of $LaCrO_3$.

The crystalline structure analysis using XRD pattern is shown in Figure 4. A single orthorhombic structure of Pnma space group was identified (JCPD #000330701). The Rietveld refinement of X-ray diffraction pattern shows that $LaCrO_3$ compound has the following lattice parameters: a = 5.56 Å, b = 7.85 Å and c = 5.55 Å, corresponding to a cell volume of 342.62 Å$^3$ (Figure 4). The profile reliability factors Rp = 5.68 and Rwp = 7.38 show a good fit between the calculated diagram and the observed data. The results are in

adequation with those of the orthorhombic (pnma space group) perovskite-type oxides of the lanthanum chromite [44].
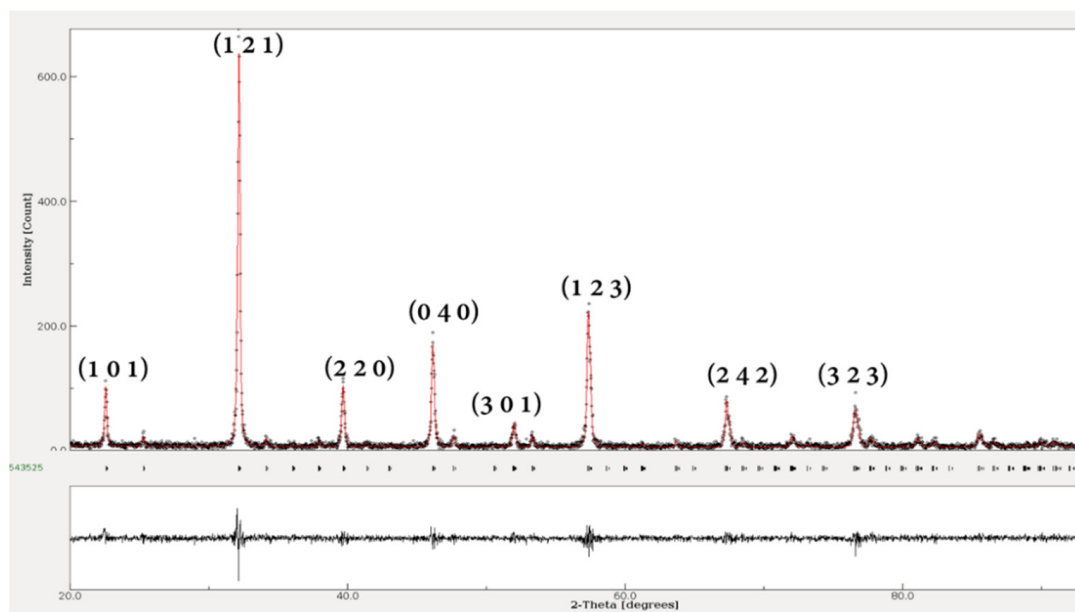


**Figure 4.** XRD and refinement pattern of LaCrO$_3$.

SEM micrographs of the powder are presented in Figure 5 before and after hydrogenation of the compound LaCrO$_3$. The powder from the sol-gel process is irregularly shaped, non-spherical and its particles are less than 18 μm. The appearance of cracks due to hydrogen embrittlement during the hydrogenation phase was observed. In addition, grain distribution was similar after hydrogenation. EDX analysis, Figure 6 shows that the peaks corresponding to constituent elements (La, Cr and O) exist in amounts corresponding to LaCrO$_3$ composition. The powder resulting from the Pechini sol-gel process was irregular in shape, not spherical, and its particles have a size of less than 18 μm.
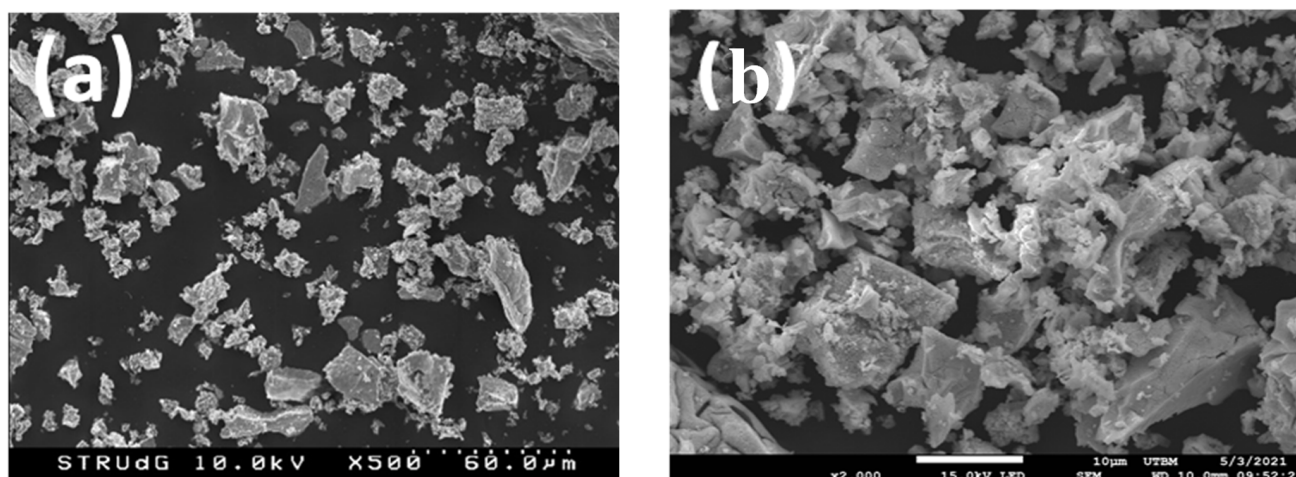


**Figure 5.** Field Emission Scanning Electron Micrographs of LaCrO$_3$ before and after hydrogenation (**a**,**b**) respectively.
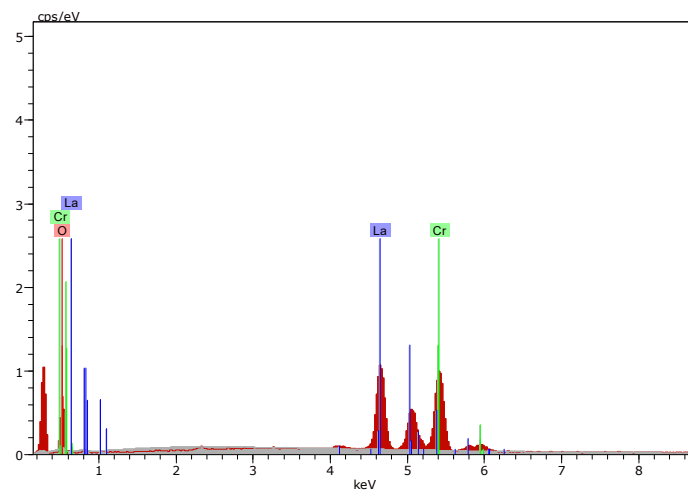
**Figure 6.** EDX spectra of LaCrO$_3$.

The pressure-composition temperature (PCT) curves for hydrogen absorption and desorption for LaCrO$_3$ were generated at three temperatures: 298 K, 313 K and 333 K. PCT curves in Figure 7a show that this hydride exhibits a single plateau at all experimental temperatures.
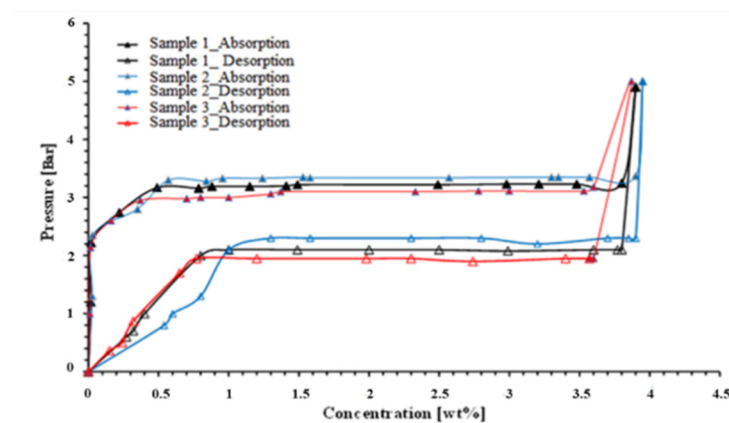


(**a**)
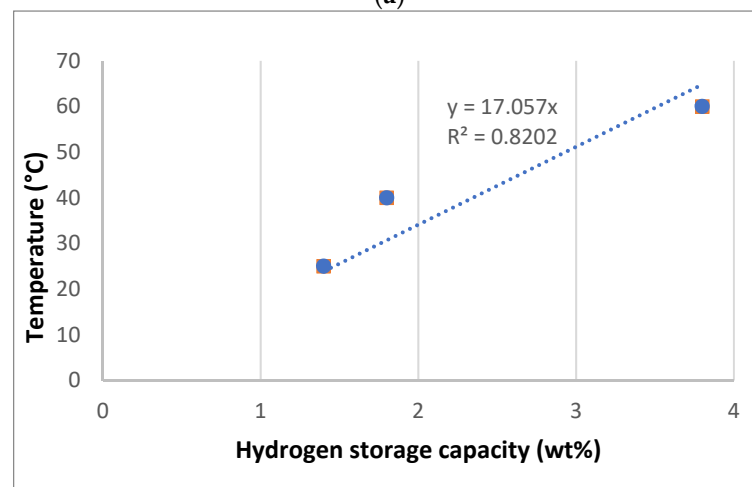


(**b**)

**Figure 7.** (**a**) PCT Curves of LaCrO$_3$ at 333 K, (**b**) Evolution of hydrogen storage with temperature.

Comparing PCT results, the three samples of the LaCrO$_3$ compound show almost the same hydrogen sorption and desorption capacities and they all show a hydrogen storage capacity up to 4 wt% under 333 K. Thus, each sample has trays, one for absorption and the second for desorption. At 303 K, the samples tested have the lowest storage capacity. The maximum storage capacity increases from 1.2 wt% to almost 4 wt% at 333 K. This variation can be explained by the fact that the compound is not stressed at its absorption and desorption temperature. In addition, Figure 7b represents the trend of the evolution of hydrogen storage properties with temperature increasing.

Besides, hydrogen storage capacity varies from 1.4 wt% at room temperature to almost 4 wt% at 333 K (60 °C), which shows the ability of this oxide to store hydrogen at a very moderate temperature. The storage capacity is comparable to that of perovskite hydrides, such as CaCoH$_3$ (2.97 wt%), CaFeH$_3$ (3.06 wt%), CaMnH$_3$ (3.09 wt%), MgCuH$_3$ (3.32 wt%) and MgNiH$_3$ (3.51 wt%) [45,46]. Additionally, compared to some other hydrides of the AB and AB$_5$ families used for solid hydrogen storage, LaCrO$_3$ perovskite oxides present better storage capacities, which allowed to promote their use for future transportation applications. Indeed, TiFe, which is the typical compound of the AB family, has a maximum mass capacity of hydrogen storage of 1.8 wt% [47]. In addition, LaNi$_5$, the typical compound of AB$_5$, presents a maximum storage capacity of 1.49 wt% [48]. Thus, LaCrO$_3$ shows good hydrogen storage properties and might be considered for transportation application in the future.

## 4. Conclusions

In this study, ab-initio calculations were performed in order to study the perovskite-type oxide LaCrO$_3$ for hydrogen storage applications. The mechanical stability reveals that LaCrO$_3$H$_6$ is thermodynamically stable. Cell parameters, crystal structures and mechanical properties were in the range of literature data when possible. The numerical part of this paper showed the utility of ab-initio calculations in order to study a compound for hydrogen storage. In addition, LaCrO$_3$ perovskite prepared by sol-gel Pechini method has shown the presence of a single-phase perovskite oxide with an orthorhombic structure. Before calcination of the compound, thermogravimetric analysis was conducted to determine the calcination temperature. XRD analysis was conducted with the aim of understanding the structural properties of the compound. Furthermore, morphology and thermal analysis of the structure have also been discussed. Hydrogen absorption/desorption PCT measurements on LaCrO$_3$ compound exhibits a single plateau at all experimental temperatures. Finally, LaCrO$_3$ compound shows a good hydrogen storage capacity of about 4 wt%, which is higher than traditional alloys used for hydrogen storage. Additionally, this study gives a good insight for further investigations on this type of compound.

**Author Contributions:** Conceptualization, M.A.L.N.; methodology, M.A.L.N.; investigation, M.A.L.N.; resources, N.F. and J.J.S.; writing—original draft preparation, M.A.L.N. and N.F.; writing—review and editing, M.A.L.N., N.F., I.P. and J.J.S.; visualization, N.F., I.P. and J.J.S.; supervision, N.F., I.P. and J.J.S.; project administration, N.F. and J.J.S. All authors have read and agreed to the published version of the manuscript.

**Institutional Review Board Statement:** Not applicable.

**Informed Consent Statement:** Not applicable.

**Data Availability Statement:** Not applicable.

**Conflicts of Interest:** The authors declare that they have no conflict of interest.

## References

1. Baysal, M.B.; Surucu, G.; Deligoz, E.; Ozısık, H. The effect of hydrogen on the electronic, mechanical and phonon properties of LaMgNi$_4$ and its hydrides for hydrogen storage applications. *Int. J. Hydrogen Energy* **2018**, *43*, 23397–23408. [CrossRef]
2. Afzal, M.; Mane, R.; Sharma, P. Heat transfer techniques in metal hydride hydrogen storage: A review. *Int. J. Hydrogen Energy* **2017**, *42*, 30661–30682. [CrossRef]
3. Chen, Y.; Dai, J.; Song, Y. Stability and hydrogen adsorption properties of Mg/Mg$_2$Ni interface: A first principles study. *Int. J. Hydrogen Energy* **2018**, *43*, 16598–16608. [CrossRef]
4. Ćirić, K.D.; Koteski, V.J.; Stojić, D.L.j.; Radakovic, J.S.; Ivanovski, V.N. HfNi and its hydrides—First principles calculations. *Int. J. Hydrogen Energy* **2010**, *35*, 3572–3577. [CrossRef]
5. Wang, F.; Zhang, T.; Hou, X.; Zhang, W.; Tang, S.; Sun, H.; Zhang, J. Li-decorated porous graphene as a high-performance hydrogen storage material: A first-principles study. *Int. J. Hydrogen Energy* **2017**, *42*, 10099–10108. [CrossRef]
6. Sharma, A. Investigation on platinum loaded multi-walled carbon nanotubes for hydrogen storage applications. *Int. J. Hydrogen Energy* **2020**, *45*, 2967–2974. [CrossRef]
7. Abe, J.O.; Popoola, A.P.I.; Ajenifuja, E.; Popoola, O.M. Hydrogen energy, economy and storage: Review and recommendation. *Int. J. Hydrogen Energy* **2019**, *44*, 15072–15086. [CrossRef]
8. ullah Rather, S. Preparation, characterization and hydrogen storage studies of carbon nanotubes and their composites: A review. *Int. J. Hydrogen Energy* **2020**, *45*, 4653–4672. [CrossRef]
9. Sreedhar, I.; Kamani, K.M.; Kamani, B.M.; Reddy, B.M.; Venugopal, A. A Bird's Eye view on process and engineering aspects of hydrogen storage. *Renew. Sustain. Energy Rev.* **2018**, *91*, 838–860. [CrossRef]
10. Shiraz, H.G.; Tavakoli, O. Investigation of graphene-based systems for hydrogen storage. *Renew. Sustain. Energy Rev.* **2017**, *74*, 104–109. [CrossRef]
11. Sadhasivam, T.; Kim, H.-T.; Jung, S.; Roh, S.-H.; Park, J.-H.; Jung, H.-Y. Dimensional effects of nanostructured Mg/MgH$_2$ for hydrogen storage applications: A review. *Renew. Sustain. Energy Rev.* **2017**, *72*, 523–534. [CrossRef]
12. Mori, D.; Hirose, K. Recent challenges of hydrogen storage technologies for fuel cell vehicles. *Int. J. Hydrogen Energy* **2009**, *34*, 4569–4574. [CrossRef]
13. Kukkapalli, V.K.; Kim, S. Optimization of Internal Cooling Fins for Metal Hydride Reactors. *Energies* **2016**, *9*, 447. [CrossRef]
14. Baptista, A.; Pinho, C.; Pinto, G.; Ribeiro, L.; Monteiro, J.; Santos, T. Assessment of an Innovative Way to Store Hydrogen in Vehicles. *Energies* **2019**, *12*, 1762. [CrossRef]
15. Irshad, M.; ul Ain, Q.; Siraj, K.; Raza, R.; Tabish, A.N.; Rafique, M.; Idrees, R.; Khan, F.; Majeed, S.; Ahsan, M. Evaluation of BaZr$_{0.8}$X$_{0.2}$ (X = Y, Gd, Sm) proton conducting electrolytes sintered at low temperature for IT-SOFC synthesized by cost effective combustion method. *J. Alloy. Compd.* **2020**, *815*, 152389. [CrossRef]
16. Sun, C.; Alonso, J.A.; Bian, J. Recent Advances in Perovskite-Type Oxides for Energy Conversion and Storage Applications. *Adv. Energy Mater.* **2021**, *11*, 2000459. [CrossRef]
17. Butenko, D.S.; Li, S.; Kotsyubynsky, V.O.; Boychuk, V.M.; Dubinko, V.I.; Kolkovsky, P.I.; Liedienov, N.A.; Klyui, N.I.; Han, W.; Zatovsky, I.V. Palladium nanoparticles embedded in microporous carbon as electrocatalysts for water splitting in alkaline media. *Int. J. Hydrogen Energy* **2021**, *46*, 21462–21474. [CrossRef]
18. Wei, Z.; Pashchenko, A.V.; Liedienov, N.A.; Zatovsky, I.V.; Butenko, D.S.; Li, Q.; Fesych, I.V.; Turchenko, V.A.; Zubov, E.E.; Polynchuk, P.Y.; et al. Multifunctionality of lanthanum–strontium manganite nanopowder. *Phys. Chem. Chem. Phys.* **2020**, *22*, 11817–11828. [CrossRef]
19. Young, K.-H. Research in Nickel/Metal Hydride Batteries 2016. *Batteries* **2016**, *2*, 31. [CrossRef]
20. Liu, W.; Webb, C.J.; Gray, E.M. Review of hydrogen storage in AB3 alloys targeting stationary fuel cell applications. *Int. J. Hydrogen Energy* **2016**, *41*, 3485–3507. [CrossRef]
21. Inoue, H.; Kotani, N.; Chiku, M.; Higuchi, E. Ti–V–Cr–Ni alloys as high capacity negative electrode active materials for use in nickel–metal hydride batteries. *Int. J. Hydrogen Energy* **2016**, *41*, 9939–9947. [CrossRef]
22. Hydrogen Storage in MgX (X = Cu and Ni) Systems—Is There Still News?—ScienceDirect. Available online: https://www.sciencedirect.com/science/article/pii/S0378775318310140 (accessed on 31 November 2021).
23. First-Principles Calculations of Structural, Elastic, Electronic, and Optical Properties of Perovskite-Type KMgH3 Crystals: Novel Hydrogen Storage Material | The Journal of Physical Chemistry B. Available online: https://pubs.acs.org/doi/10.1021/jp111382h (accessed on 31 November 2021).
24. Ikeda, K.; Kato, S.; Ohoyama, K.; Nakamori, Y.; Takeshita, H.T.; Orimo, S. Formation of perovskite-type hydrides and thermal desorption processes in Ca–T–H (T=3d transition metals). *Scr. Mater.* **2006**, *55*, 827–830. [CrossRef]
25. Dutta, S. A review on production, storage of hydrogen and its utilization as an energy resource. *J. Ind. Eng. Chem.* **2014**, *20*, 1148–1156. [CrossRef]
26. Pottmaier, D.; Pinatel, E.R.; Vitillo, J.G.; Garroni, S.; Orlova, M.; Baró, M.D.; Vaughan, G.B.M.; Fichtner, M.; Lohstroh, W.; Baricco, M. Structure and Thermodynamic Properties of the NaMgH3 Perovskite: A Comprehensive Study. *Chem. Mater.* **2011**, *23*, 2317–2326. [CrossRef]
27. Bouhadda, Y.; Bououdina, M.; Fenineche, N.; Boudouma, Y. Elastic properties of perovskite-type hydride NaMgH$_3$ for hydrogen storage. *Int. J. Hydrogen Energy* **2013**, *38*, 1484–1489. [CrossRef]

28. Sakaguchi, H.; Hatakeyama, K.; Kobayashi, S.; Esaka, T. Hydrogenation characteristics of the proton conducting oxide–hydrogen storage alloy composite. *Mater. Res. Bull.* **2002**, *37*, 1547–1556. [CrossRef]

29. Esaka, T.; Sakaguchi, H.; Kobayashi, S. Hydrogen storage in proton-conductive perovskite-type oxides and their application to nickel–hydrogen batteries. *Solid State Ion.* **2004**, *166*, 351–357. [CrossRef]

30. Deng, G.; Chen, Y.; Tao, M.; Wu, C.; Shen, X.; Yang, H.; Liu, M. Study of the electrochemical hydrogen storage properties of the proton-conductive perovskite-type oxide LaCrO3 as negative electrode for Ni/MH batteries. *Electrochim. Acta* **2010**, *55*, 884–886. [CrossRef]

31. Gencer, A.; Surucu, G.; Al, S. MgTiO$_3$H$_x$ and CaTiO$_3$H$_x$ perovskite compounds for hydrogen storage applications. *Int. J. Hydrogen Energy* **2019**, *44*, 11930–11938. [CrossRef]

32. Hohenberg, P.; Kohn, W. Inhomogeneous Electron Gas. *Phys. Rev.* **1964**, *136*, B864–B871. [CrossRef]

33. Kohn, W.; Sham, L.J. Self-Consistent Equations Including Exchange and Correlation Effects. *Phys. Rev.* **1965**, *140*, A1133–A1138. [CrossRef]

34. Perdew, J.P.; Burke, K.; Ernzerhof, M. Generalized Gradient Approximation Made Simple. *Phys. Rev. Lett.* **1996**, *77*, 3865–3868. [CrossRef] [PubMed]

35. Schwarz, K.; Blaha, P.; Madsen, G.K.H. Electronic structure calculations of solids using the WIEN2k package for material sciences. *Comput. Phys. Commun.* **2002**, *147*, 71–76. [CrossRef]

36. Lutterotti, L.; Dell'Amore, F.; Angelucci, D.E.; Carrer, F.; Gialanella, S. Combined X-ray diffraction and fluorescence analysis in the cultural heritage field. *Microchem. J.* **2016**, *126*, 423–430. [CrossRef]

37. Song, Q.; Du, Q.; Song, L.; Zhao, H.; Guo, Y. The Structural Stabilities and Electronic Properties of Orthorhombic and Rhombohedral LaCrO$_3$—A First-Principles Study. *Int. J. Nanomanuf.* **2014**, *10*, 13–25. [CrossRef]

38. Murnaghan, F.D. The Compressibility of Media under Extreme Pressures. *Proc. Natl. Acad. Sci. USA* **1944**, *30*, 244–247. [CrossRef]

39. Parey, V.; Shukla, A.; Parveen, A.; Bano, A.; Khare, P.; Gaur, N.K. Thermal properties of solid oxide fuel cell perovskite LaCrO$_3$. *AIP Conf. Proc.* **2016**, *1728*, 020026. [CrossRef]

40. Wang, Z.; Shi, X.; Yang, X.-S.; Liu, Z.; Shi, S.-Q.; Ma, X. The Effects of Hydrogen Distribution on the Elastic Properties and Hydrogen-Induced Hardening and Softening of α-Fe. *Appl. Sci.* **2020**, *10*, 8958. [CrossRef]

41. Soltani, N.; Hosseini, S.M.; Kompany, A. Nanoscale ab-initio calculations of optical and electronic properties of LaCrO3 in cubic and rhombohedral phases. *Phys. B Condens. Matter* **2009**, *404*, 4007–4014. [CrossRef]

42. Huang, Z.W.; Zhao, Y.H.; Hou, H.; Han, P.D. Electronic structural, elastic properties and thermodynamics of Mg$_{17}$Al$_{12}$, Mg$_2$Si and Al$_2$Y phases from first-principles calculations. *Phys. B Condens. Matter* **2012**, *407*, 1075–1081. [CrossRef]

43. Aamir, M.; Bibi, I.; Ata, S.; Majid, F.; Kamal, S.; Alwadai, N.; Sultan, M.; Iqbal, S.; Aadil, M.; Iqbal, M. Graphene oxide nanocomposite with Co and Fe doped LaCrO$_3$ perovskite active under solar light irradiation for the enhanced degradation of crystal violet dye. *J. Mol. Liq.* **2021**, *322*, 114895. [CrossRef]

44. Khattak, C.P.; Cox, D.E. Structural studies of the (La, Sr)CrO/sub 3/ system. *Mater. Res. Bull. (USA)* **1977**, *12*, 463–471. [CrossRef]

45. Al, S.; Iyigor, A. Structural, electronic, elastic and thermodynamic properties of hydrogen storage magnesium-based ternary hydrides. *Chem. Phys. Lett.* **2020**, *743*, 137184. [CrossRef]

46. Surucu, G.; Gencer, A.; Candan, A.; Gullu, H.H.; Isik, M. CaXH$_3$ (X = Mn, Fe, Co) perovskite-type hydrides for hydrogen storage applications. *Int. J. Energy Res.* **2020**, *44*, 2345–2354. [CrossRef]

47. Yukawa, H.; Takahashi, Y.; Morinaga, M. Electronic structures of hydrogen storage compound, TiFe. *Comput. Mater. Sci.* **1999**, *14*, 291–294. [CrossRef]

48. Liang, L.; Yang, Q.; Zhao, S.; Wang, L.; Liang, F. Excellent catalytic effect of LaNi5 on hydrogen storage properties for aluminium hydride at mild temperature. *Int. J. Hydrogen Energy* **2021**, *46*, 38733–38740. [CrossRef]